



## Comparative study of the efficiency of Au, Ag, Pd and Pt based mono and bimetallic trimer clusters for the CO oxidation reaction

Saumya Gurtu<sup>a</sup>, Sandhya Rai<sup>b</sup> and U. Deva Priyakumar<sup>a\*</sup>

<sup>a</sup>Center for Computational Natural Sciences and Bioinformatics, International Institute of Information Technology, Hyderabad-500 032, India

<sup>b</sup>Theoretical Science Unit, Jawaharlal Nehru Centre for Advanced Scientific Research, Jakkur, Bengaluru-560 001, India

E-mail: deva@iiit.ac.in

Manuscript received online 29 April 2019, revised and accepted 23 May 2019

Understanding synergistic effect by calculating electronic structure is essential to fine-tune the catalytic properties of bimetallic nanoalloy clusters which might be used for design of novel efficient catalysts. Density functional theory PBE0 calculations were performed to investigate the structure and energetics of various intermediates involved in the CO oxidation reaction catalyzed by  $Au_{3-x}Y_x$  ( $x = 0-3$  and Y denotes Ag or, Pt or, Pd) trimeric clusters through two possible pathways: Eley-Rideal (ER) and Langmuir-Hinshelwood (LH). The results of this investigation show that the catalytic behavior of the nanocluster highly depends on its composition and the reaction site taken into consideration. The most active reaction centres of gold-silver, gold-palladium, gold-platinum clusters are gold, palladium and platinum atoms respectively. The gold-silver clusters and  $AuPt_2$  prefer ER mechanism whereas, gold-palladium and  $Au_2Pt$  selectively favour LH mechanism in comparison to the other. Bimetallic clusters, in general, are more efficient in comparison to their pristine mono-metallic counterparts, in activating the O-O bond for the reaction and have relatively easy  $CO_2$  dissociation. Overall results indicate that the alloyed clusters could potentially have a better catalytic activity as compared to pure gold clusters for CO oxidation at low temperatures.

Keywords: CO oxidation, heterogeneous catalysis, reaction mechanism, nanocluster composition, dopant, synergistic effects, Eley-Rideal (ER), Langmuir-Hinshelwood (LH).

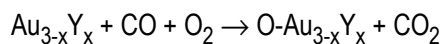
### 1. Introduction

Nanosized (< 5 nm) transition metal gold, although a noble metal, has been reported to be a good heterogeneous catalyst for a number of oxidation reactions at low temperatures (200–350 K)<sup>1–5</sup>. Haruta *et al.* were the first to explore the latent qualities of supported nano gold clusters in catalyzing the carbon monoxide oxidation process at low temperatures<sup>1</sup>. Later, many research studies have reported the catalytic properties of gold nanoclusters<sup>5–16</sup>. Herzing *et al.*<sup>17</sup> also gave an experimental evidence of catalysis by subnanometer species of ~10 Au atoms for carbon monoxide oxidation reaction. It was demonstrated in certain studies that anionic gold dimer is the smallest gold cluster that can catalyse CO oxidation reaction<sup>18,19</sup>. Two different mechanisms for the reaction were proposed, one with a carbonate like intermediate and the other via peroxyformate like intermediate. There are studies of similar nanosize catalytic effects for silver<sup>20–24</sup>,

platinum<sup>25</sup> and palladium<sup>26</sup> clusters as well. So for almost three decades, metal clusters seem to be propitious models for new surface catalytic materials.

The principal facet in the catalysis of the carbon monoxide oxidation is the activation of O-O bond<sup>27</sup>. Though CO is easily adsorbed on gold nanoparticles but, the oxygen molecules are neither strongly adsorbed nor activated<sup>28,29</sup>. One way to solve this issue is to use the oxide support which usually plays a significant role in the activation of oxygen<sup>27–30</sup>. The other way can be making an active catalyst by alloying gold nanoparticles with a metal of stronger reduction tendency<sup>31,32</sup>. This will cause stronger electron transfer to oxygen as well as a good CO adsorption. Earlier, Wöste *et al.*<sup>33</sup> examined the CO oxidation catalysis by gold-palladium bimetallic nanoparticles supported on  $SiO_2$ , but did not observe synergistic effect compared to the performance of monometallic catalyst in their case which they explained by

the strong oxygen adsorption by palladium. Iizuka *et al.*<sup>34</sup> found that silver impurity in gold nanoparticles augments the reaction of CO oxidation and the degree of augmentation strongly correlates with the silver content on surface. The works of Liu *et al.*<sup>31</sup> and Negreiros *et al.*<sup>35</sup> on supported gold-silver alloy systems both report that there is a strong synergistic effect in their high catalytic activity with silver playing a key role in the activation of oxygen. Wang *et al.*<sup>36</sup> also analysed the potential activity of gold-platinum tetramers for CO oxidation and suggested that Pt sites are the catalytically active centers in such alloys and reaction site is also very important for such systems. In addition to CO oxidation reaction, previous studies have shown that reaction rates can be accelerated by using nanoalloys as catalysts<sup>37–40</sup>. In this paper, we consider a total of six unsupported bimetallic trimers along with four pristine clusters, with each atom of cluster having the same coordination number. One of the reasons to consider unsupported metal clusters in the gas phase for this paper is that we want to concentrate on the intrinsic metal effects, i.e. no incorporation of possible auxiliary effects of a support<sup>41–43</sup>. Although such effects may be relevant, to first substantiate the presence of intrinsic metal effects<sup>44,45</sup> is worthwhile, specifically when it has been discovered experimentally that nano gold structures with no support are also good catalysts<sup>46,47</sup>. The other reason is that such exhaustive theoretical studies delineating the reaction mechanism involving metal cluster catalysts have rarely been conducted<sup>48–52</sup>. The scope of this paper is confined to the analysis of the first part of CO oxidation reaction only where a nascent oxygen binds to the catalyst, that eventually gets released on the oxidation with the second molecule of CO. This reaction in presence of the catalysts considered in this paper can be formulated as follows:



We choose to analyse the above reaction by the two most plausible surface reaction mechanisms – one via formation of peroxy type TS (Eley-Rideal) and the other via formation of a superoxy type TS (Langmuir-Hinshelwood) given by ER pathways and LH pathways respectively in this paper. In LH mechanism<sup>53–59</sup> two molecules adsorb on neighboring sites and the adsorbed molecules undergo a bimolecular reaction whereas, in ER mechanism only one of the molecules adsorbs and the other one reacts with it directly from the gas phase, without adsorbing<sup>18,60</sup>. We have also used these mechanism definitions for our earlier work of benchmarking of DFT

functionals for the same CO oxidation reaction<sup>16,61</sup>. The highlight of this thorough analysis is that we compare the catalytic activities of a variety of transition noble metals and their combinations as trimers with precise reaction mechanisms for CO oxidation.

To the best of our knowledge, no such detailed systematic study of carbon monoxide oxidation reaction on such bimetallic trimers is available yet. A comprehensive theoretical inspection of the potential energy surface for CO oxidation reaction on unsupported bimetallic and monometallic trimers has been performed and the relative studies are presented in this paper to give a deep insight into the intrinsic metal effects on the reaction mechanism.

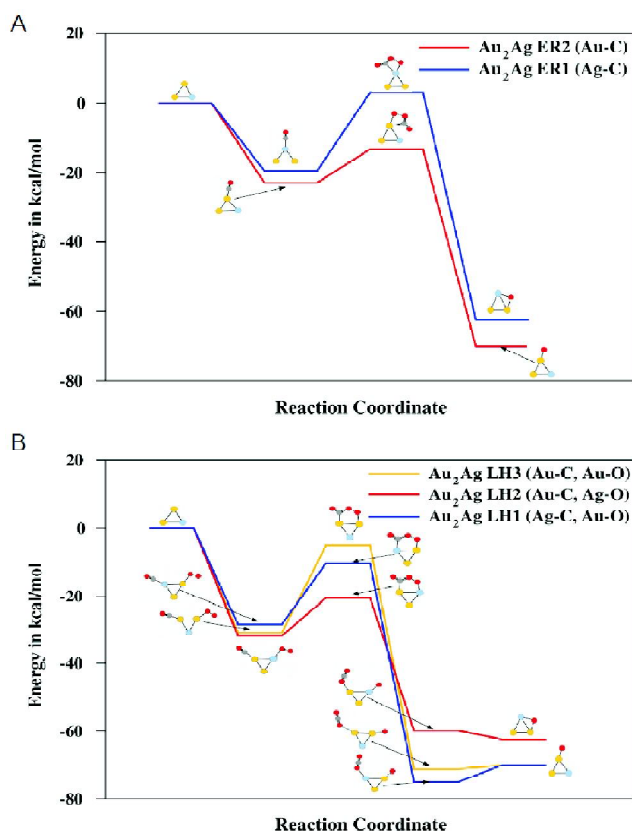


**Fig. 1.** Potential energy surfaces for CO oxidation catalyzed by  $\text{Au}_2\text{Ag}$  cluster. The corresponding intermediates and transition states related to pathways are also presented. The sum of energies of free  $\text{Au}_2\text{Ag}$ , CO and  $\text{O}_2$  is set to zero as a reference. All energies are in kcal/mol. (A) The two possible ER mechanisms: The blue line represents the PES for mechanism via CO adsorption at Ag (blue) atom while the red one represents the mechanism in which CO is adsorbed at Au (yellow) atom. (B) The three possible LH mechanisms with different CO and  $\text{O}_2$  adsorption sites. Each different combinations of adsorption sites are labeled as (Ag-C, Au-O), (Au-C, Ag-O), (Au-C, Au-O) and marked by different colors.

## 2. Methods

Previous benchmarking evaluations have shown that the exchange-correlation DFT functional of Perdew, Burke and Ernzerhof (PBE0)<sup>4,61–63</sup> was sufficiently accurate for describing noble-metal systems<sup>11,64–67</sup>. PBE0 was also shown to be adequate for CO oxidation on Au<sub>3</sub> cluster. All the calculations reported here were performed using the PBE0 functional using the Gaussian 09 suite of programs<sup>68</sup>. Stuttgart-Dresden (SDD) double- $\zeta$  basis set was used to model the valence electrons explicitly and the corresponding SDD relativistic effective core potential<sup>69–72</sup> was used to model the core electrons for the metals<sup>73</sup>. The introduction of effective core potential also reduces the basis set superposition error (BSSE)<sup>74–76</sup> in the calculations. The keyword “5d” is also used in conjunction with the basis set keywords to use five pure d functions in the calculations. We used the 6-31+G(d) split-valence Pople basis set for the carbon and oxygen atoms, which includes single polarization and diffuse functions.

No symmetry constraints were used in the geometry optimization calculations. The vibrational frequency calculations were done to verify the nature of different stationary points found on the potential energy surfaces. These stationary points were identified as either minima with no imaginary frequency or TS with one imaginary frequency. Then, to identify the minima connected through the transition state we use Gonzalez-Schlegel method for intrinsic reaction coordinate (IRC) calculations<sup>58</sup>. Lowest spin states were considered for all the clusters.

## 3. Results and discussion

The d-d and s-d interaction between dopants and gold atoms can modify the electronic properties of clusters which may alter their interaction with the incoming O<sub>2</sub>, CO and CO<sub>2</sub> molecules<sup>77–79</sup>. Thus, the intent is to elucidate composition and reaction site dependency of cluster reactivity for CO oxidation reaction and to compare the catalytic behaviour of gold-based clusters with monometallic gold trimer Au<sub>3</sub>. Fig. 1 shows all the possible potential energy surfaces for CO oxidation reaction catalyzed by Au<sub>2</sub>Ag cluster through (A) ER mechanisms and (B) LH mechanisms. The potential energy surface for this reaction catalyzed by other clusters considered in the paper are given in the Supplementary material.

### 3.1. Analysis of different reaction sites of bimetallic clusters

There are two possible pathways to study reaction catalyzed by pure clusters – one ER pathway and one LH pathway. But for bimetallic clusters, we have two ER pathways – one with CO adsorption at Au site and the other with CO adsorption at Y site and three LH pathways – one with Au-Y site with CO adsorbed at Au (labeled as Au-C, Y-O), the other with Au-Y site with CO adsorbed at Y (labeled as Y-C, Au-O) and, the third with Au-Au (labeled as Au-C, Au-O) site for singly doped whereas Y-Y site for doubly doped clusters (labeled as Y-C, Y-O) as shown in Fig. 2. CO adsorption at A

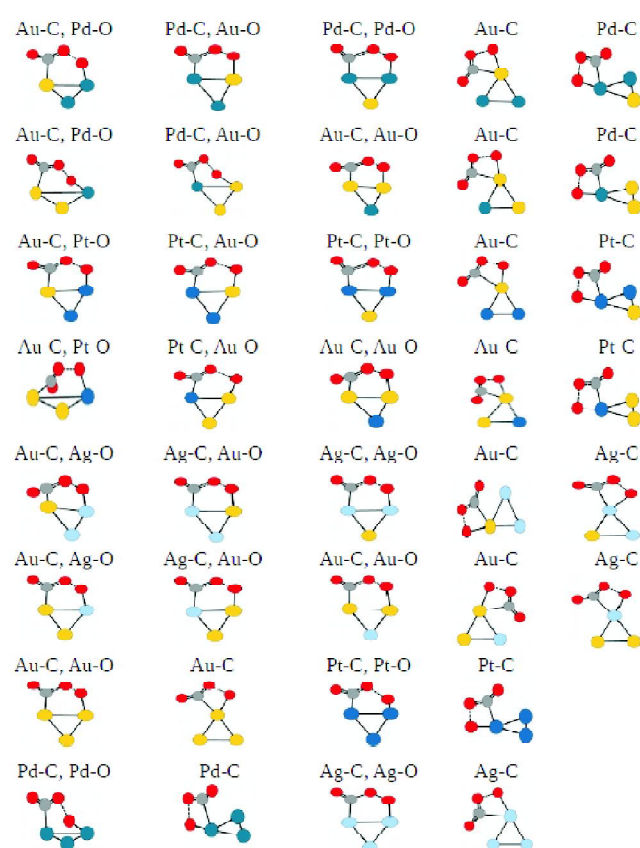


**Fig. 2.** Various possible reaction sites for Au, Ag, Pt and Pd based mono/bimetallic clusters.

atom is denoted by A-C where, C is for carbon atom and O<sub>2</sub> adsorption at B atom is indicated by B-O where, O symbolizes oxygen atom. The atom at which CO is adsorbed in case of ER mechanism and the combination of atoms at which CO and O<sub>2</sub> are co-adsorbed on cluster in case of LH mechanism show different behavior towards various properties of reaction pathway. Just like in case of transition state with gold cluster as catalyst, most of the transition states with

bimetallic clusters are thermodynamically more stable than the isolated reactants of the given reaction as shown in Fig. 3. It is important to mention here that the reference energy  $E(\text{Ref})$  is taken to be the sum of energies of isolated reactants – corresponding cluster, CO and  $\text{O}_2$ , for this analysis. Fig. 3 shows that the reaction can be catalyzed by most of the bimetallic clusters at ambient temperatures. The bimetallic clusters of gold-silver, gold-palladium, gold-platinum have transition states with CO adsorption occurring at Au, Pd and Pt atoms respectively for ER mechanism as the most energetically favorable ones. In case of LH mechanism, singly doped clusters show the most energetically favorable TS obtained when the reaction occurs at (Au-C, Ag-O) site for gold-silver clusters, (Au-O, Pd-C) site for gold-palladium clusters and (Au-O, Pt-C) site for gold-platinum clusters. In contrast to this, (Y-C, Y-O) reaction site for doubly doped clusters gives energetically most favourable transition state.

But there are a few reaction sites which show positive values of transition state energy with respect to energy of isolated reactants. For a few ER pathways, this TS energy value with respect to the corresponding reference is positive for  $\text{Au}_2\text{Ag}$  at Ag site,  $\text{Au}_2\text{Pd}/\text{Au}_2\text{Pt}$  at Au site and  $\text{AuPd}_2/\text{AuPt}_2$  at Au site and that gives rise to high activation energy barrier for those pathways. Similarly, the energy of TS with respect to its reference is positive for LH pathway via (Au-C, Au-O) site in case of both  $\text{Au}_2\text{Pd}$  and  $\text{Au}_2\text{Pt}$  clusters. This shows that CO adsorption on gold atom and co-adsorption of CO and  $\text{O}_2$  over Au-Au side of cluster reduces the catalytic efficiency of gold-palladium and gold-platinum trimers (refer Supplementary material for the PES). Hence, reaction site is very critical for a designed cluster to avoid the possibility of the reaction to take place via another pathway with a higher barrier height.

The  $\text{CO}_2$  dissociation energy is also calculated for each reaction pathway by subtracting the energy of final products of half reaction (cluster with a nascent O attached and  $\text{CO}_2$ ) from the energy of the Intermediate where  $\text{CO}_2$  is formed on the cluster (Int2). The reaction pathway for  $\text{Ag}_3$  has no energy barrier for  $\text{CO}_2$  dissociation and the gold-silver trimers also show very low or no  $\text{CO}_2$  dissociation energy barriers when CO is adsorbed at Au site. Most of the gold-palladium and gold-platinum clusters have very low  $\text{CO}_2$  dissociation energy as compared to monometallic counterparts (refer Table 1), especially when CO is adsorbed at Au atom. Lesser  $\text{CO}_2$  dissociation energy is endorsed by long metal- $\text{CO}_2$  bond

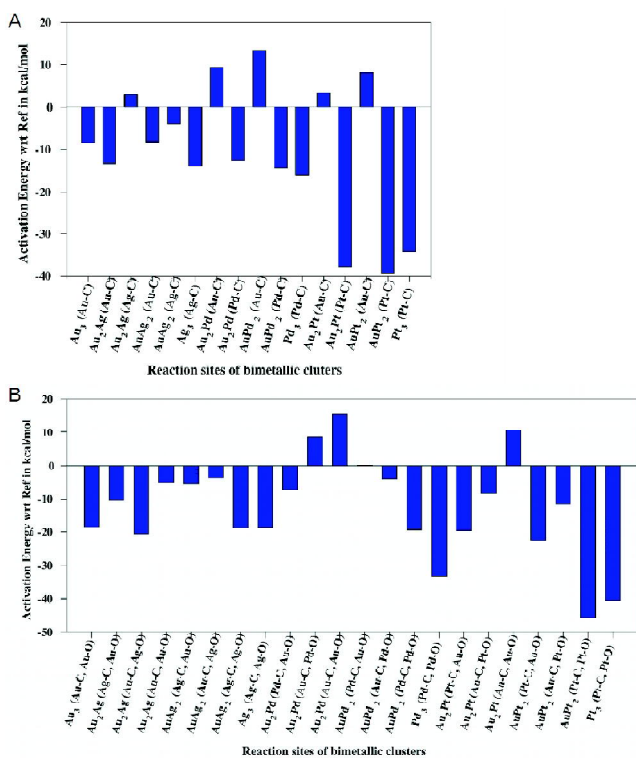


**Fig. 3.** The difference of energy (in kcal/mol) of the transition state  $E(\text{TS})$  and the reference given by  $E(\text{TS})-E(\text{Ref})$  is analyzed for both (A) ER and (B) LH mechanisms on all clusters. The positive values in the figure show that the energy for such TS is higher with respect to the energy of corresponding isolated reactants and the negative values indicate that the corresponding TS is lower in energy with respect to the energy of isolated reactants.

**Table 1.** Carbon dioxide dissociation energy values ( $E_{\text{CO}_2}$  in kcal/mol) and metal- $\text{CO}_2$  bond length ( $R_{\text{M-CO}_2}$  in Å) for CO oxidation reaction on different catalysts.  $q_{\text{transfer}}$  is the charge transfer from cluster to  $\text{CO}_2$  in a.u.

Cluster (Reaction site)	$E_{\text{CO}_2}$	$R_{\text{M-CO}_2}$	$q_{\text{transfer}}$
$\text{Au}_2\text{Ag}$ (Ag-C, Au-O)	4.95	2.43	0.29
$\text{Au}_2\text{Ag}$ (Au-C, Au-O)	1.21	2.68	0.31
$\text{AuAg}_2$ (Au-C, Ag-O)	0.72	2.76	–
$\text{AuAg}_2$ (Ag-C, Ag-O)	10.63	2.62	–
$\text{Au}_2\text{Pd}$ (Pd-C, Au-O)	3.12	2.54	0.04
$\text{Au}_2\text{Pd}$ (Au-C, Pd-O)	5.98	2.3	0.24
$\text{AuPd}_2$ (Pd-C, Au-O)	3.11	2.54	0.25
$\text{AuPd}_2$ (Au-C, Pd-O)	2.78	2.54	0.22
$\text{Au}_2\text{Pt}$ (Pt-C, Au-O)	9.71	2.24	–0.11
$\text{Au}_2\text{Pt}$ (Au-C, Pt-O)	3.76	2.45	0.42
$\text{AuPt}_2$ (Au-C, Pt-O)	3.58	2.46	0.21
$\text{AuPt}_2$ (Pt-C, Pt-O)	8.66	2.11	0.39

length, refer Table 1. The pristine clusters show strong affinity towards CO<sub>2</sub> and this is overcome by using alloyed trimers.

### 3.2. Charge analysis of transition state

According to the molecular orbital theory, HOMO of CO molecule is the high energy  $\sigma_{2p}$  which is bonding orbital whereas, LUMO is  $\pi^*_{2p}$  which are antibonding orbitals. When there is the charge transfer from a full  $\sigma$  orbital of CO to vacant d-orbitals of metal cluster, a  $\sigma$  bonding occurs. On the other hand, when there is a fully filled d-orbital of metal cluster, a back bond is formed with empty  $\pi^*$ -orbital of CO molecule, i.e. charge is transferred from metal cluster to CO molecule that strengthens the interaction between the catalyst and the reactant (CO). The comparative thermodynamic stability of a transition state of a cluster discussed in Section 3.1 can be explained qualitatively by the Mulliken charge analysis of different reaction sites for a cluster as given in Table 1. More the charge transfer from the cluster, stronger would be the bonding resulting in enhanced thermodynamic stability.

While considering the ER pathway for gold-platinum and gold-palladium clusters, Pd and Pt are the active centers of the catalyst, because of a higher interaction energy and more charge transfer from the cluster to CO. Whereas, reaction at gold atom causes gold to have higher positive charge and decreases the charge transfer significantly from the cluster. In case of gold-silver clusters, there is no significant difference in the charge transfer from the cluster when reaction takes place on Au site or Ag site but in the most stable structures, Au atoms assume positions which favor charge transfer from Ag atoms<sup>80</sup> as shown in Table 1. The preferred site in such cases is gold because d-orbitals of gold are more favorable for back donation as compared to d-orbitals of silver<sup>12</sup>. This is because of the fact that d-orbitals of silver are energetically much below their s-orbitals.

For LH pathways, combination of Au-Y works better in charge transfer from a trimer with less positive charge on gold atom as compared to Au-Au in case of singly doped clusters as shown in Table 1. Similarly, Y-Y combination in doubly doped ones causes more charge transfer from a cluster and more negative charge on gold atom owing to its higher electronegativity. The full charge analysis is given in Supplementary material.

### 3.3. Barrier height analysis

The activation energy or barrier height for the reaction is

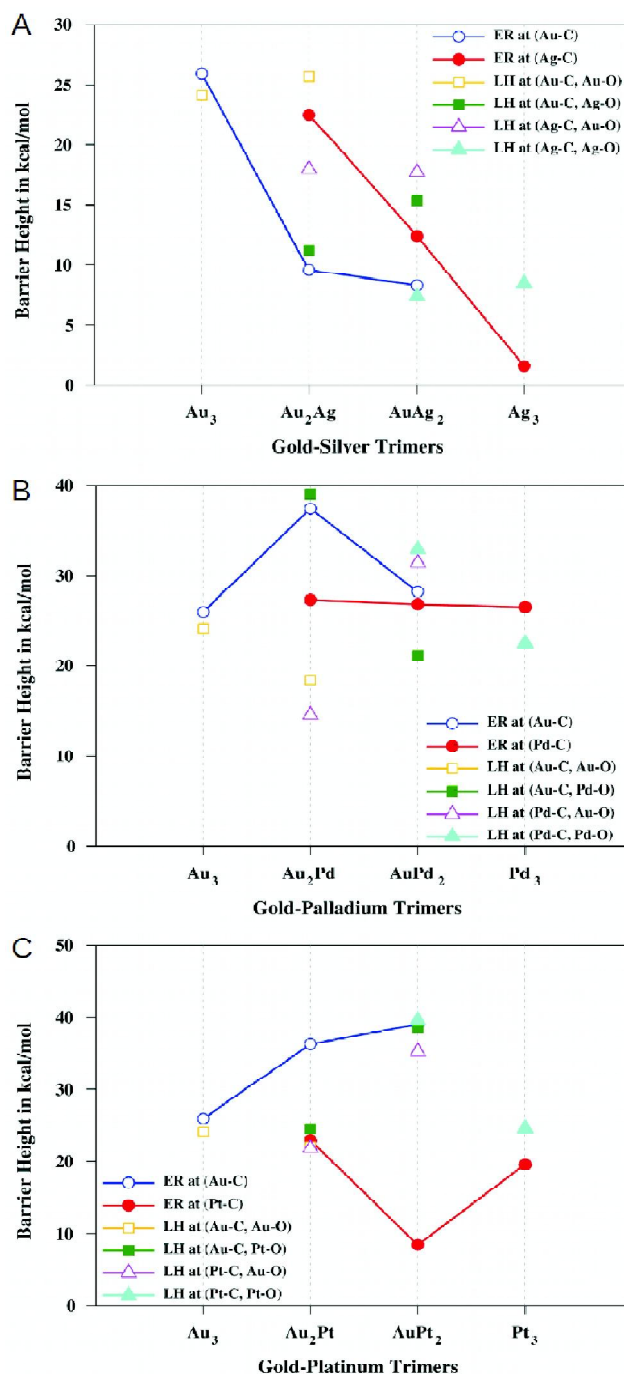


**Fig. 4.** The various barrier heights (in kcal/mol) related to respective pathways for a cluster are marked in the plot with the same x coordinate labeled by the cluster name. The various colored lines show the qualitative aspects of barrier height values of a particular reaction site with increasing content of dopant in clusters. The different colors denote various possible reaction sites.

**Table 2.** Comparison of the energetics ( $E_{ER}^{act}$  and  $E_{LH}^{act}$  in kcal/mol), charges ( $q_{ER}^{cluster}$  and  $q_{LH}^{cluster}$  in a.u.) and the geometric parameters

Clusters	$E_{ER}^{act}$	$E_{LH}^{act}$	$E_{diff}^{act}$	$(R_{ER}^{O-O}$ and $R_{LH}^{O-O}$ in Å)			
				$q_{ER}^{cluster}$	$q_{LH}^{cluster}$	$R_{ER}^{O-O}$	$R_{LH}^{O-O}$
Au <sub>3</sub>	-8.54	-18.46	9.92	0.3	0.41	1.72	1.35
Au <sub>2</sub> Ag	-13.31	-20.57	7.26	0.29	0.48	1.65	1.37
AuAg <sub>2</sub>	-8.4	-18.88	10.48	0.35	0.47	1.65	1.36
Ag <sub>3</sub>	-14.03	-18.65	4.62	0.29	0.53	1.67	1.35
Au <sub>2</sub> Pd	-12.5	-7.31	-5.19	0.24	0.32	2	1.78
AuPd <sub>2</sub>	-14.39	-19.42	5.03	0.22	0.33	1.87	1.3
Pd <sub>3</sub>	-16.02	-33.15	17.13	0.13	0.37	1.92	1.78
Au <sub>2</sub> Pt	-37.75	-19.58	-18.17	0.42	0.34	1.95	2.01
AuPt <sub>2</sub>	-39.41	-45.67	6.26	0.39	0.43	1.88	1.31
Pt <sub>3</sub>	-34.09	-40.56	6.47	0.32	0.49	1.87	1.77

given by the difference between the energy of transition state and the energy of intermediate which is mainly the energy of CO adsorbed complex with cluster and O<sub>2</sub>(g) for ER mechanism or, just the energy of CO and O<sub>2</sub> co-adsorbed complex with the cluster for LH mechanism. Table 2 clearly shows that the least barrier height possible on a bimetallic cluster is always lesser than on a pure gold cluster. We can arrive at two other important conclusions from Table 2. One is the reaction mechanism which offers the lowest barrier height for a particular cluster and the other is the cluster which performs the best among its variants with the lowest barrier height. For example, among the gold-silver variants, AuAg<sub>2</sub> with ER mechanism via Au site and LH mechanism via (Ag-C, Au-O) site perform well. For gold-palladium clusters, it is Au<sub>2</sub>Pd cluster with LH mechanism at (Pd-C, Au-O) site and AuPt<sub>2</sub> cluster with ER mechanism via CO adsorption at Pt site for gold-platinum clusters that work the best. Barrier height parameter also shows that Au, Pd, Pt atoms act as the most active centers in gold-silver, gold-palladium and gold-platinum<sup>36</sup> clusters respectively.

### 3.4. ER versus LH mechanism

LH is the favored pathway for CO oxidation reaction on a monometallic gold cluster over the ER mechanism<sup>2,16,81</sup>. The preference for LH pathway can be associated with the stability of the transition state and lesser barrier height obtained in LH pathway over the one obtained in ER pathway. The results are interesting when similar analysis is done for bimetallic clusters. The doubly doped clusters have TS from LH

mechanism more energetically favourable as compared to TS from ER mechanism by a significant energy difference (>4 kcal/mol) as shown in Table 2. Gold-silver clusters favour TS from LH mechanism more than ER TS thermodynamically with a significant energy difference. In contrast to this, gold-palladium and gold-platinum singly doped clusters have ER TS energetically more stable than the LH TS. Such a crossover of LH and ER mechanisms have been reported only in nucleobase adsorbed gold clusters<sup>16</sup>.

The charge transfer analysis from a cluster is shown in Table 2 explains that the TS state with cluster donating more electrons is more thermodynamically stable. The arrangement of charges also becomes important in the discussion of stability as explained in Section 4.1 for bimetallic nanoalloys<sup>80</sup>. As gold have higher electronegativity value as compared to other dopant atoms, the arrangement of charges with higher negative charge or lower positive charge on gold is more favourable as shown in Table 2. Therefore, ER TS is thermodynamically more favorable for Au<sub>2</sub>Pd cluster which donates more charge in case of LH TS but has a positive charge on gold atom. It is also supported by higher O-O bond activation in ER TS as shown in Table 2.

However, in case of clusters Au<sub>2</sub>Ag, AuAg<sub>2</sub> and Ag<sub>3</sub>, ER mechanism is preferred due to low barrier height and higher extent of O-O bond activation for respective ER transition states (refer  $d_{O-O}$  values in Table 2). In case of Au<sub>2</sub>Pd, AuPd<sub>2</sub> and Pd<sub>3</sub> clusters, LH mechanism is preferred due to low barrier heights and more charge transfer from the correspond-

ing cluster. The catalyst Au<sub>2</sub>Pt prefers LH mechanism whereas, AuPt<sub>2</sub> and Pt<sub>3</sub> prefer ER mechanism due to smaller barrier heights which can be interpreted from the higher activation of O-O bond as shown in Table 2. Therefore, barrier height for the reaction is the key issue that affects the ER-LH competition.

### 3.5. Cluster composition

It has already been shown in above sections that the catalytic properties of bimetallic clusters vary with the dopant type selected and its percentage in cluster composition. This is because the back donation depends on the energetic position of d-orbitals which is in turn dependent on the composition of clusters.

**3.5.1. Dopant atoms:** The most preferred reaction site for ER mechanism is Au, Pd and Pt respectively for gold-silver, gold-palladium, gold-platinum clusters which remains unaffected by dopant percentage. This is because the reaction site is one atom which does not change with increase of dopant content in cluster whereas for LH mechanism, preferred reaction site depends on dopant percentage as the possible reaction sites change with the composition. (Au-C, Ag-O) and (Pd/Pt-C, Au-O) reaction sites are preferred for singly doped clusters but for doubly doped clusters, (Y-C, Y-O) reaction site is preferred as compared to others.

Another interesting point is that the range for barrier heights for a particular bimetallic trimer over different reaction sites becomes smaller with increasing dopant content in cluster. The barrier heights for singly doped Au<sub>2</sub>Ag varies within the range of ~15 kCal/mol energy difference while for doubly doped AuAg<sub>2</sub>, it is within ~10 kCal/mol energy difference. For Au-Pd clusters, the barrier height is within the range of 24.5 kCal/mol energy difference for Au<sub>2</sub>Pd and 11.8 kCal/mol energy difference for AuPd<sub>2</sub>. Whereas, in case of Au-Pt clusters barrier height ranges within 14.5 kCal/mol energy difference for Au<sub>2</sub>Pt and 31.4 kCal/mol energy difference for Au<sub>2</sub>Pt. The range for barrier heights obtained via different reaction sites on Au<sub>2</sub>Pt is larger because the barrier height for ER mechanism at Pt atom is very low comparatively. This shows that the doubly doped clusters perform better in case of gold-silver and gold-platinum but we must be careful while considering the reaction site. Similarly, in case of gold-palladium variants, singly doped perform better if CO is adsorbed at Pd atom. Hence, based on tuning the amount of dopant in

gold nanoclusters it is possible to rationally design nanoalloys.

**3.5.2. Dopant type:** The most catalytically active centers are gold, palladium and platinum for gold-silver, gold-palladium and gold-platinum clusters. The gold-silver clusters show characters of a good catalyst with very low activation energy and negligible CO<sub>2</sub> dissociation energy. The synergistic effect of gold and silver works strongly when CO is adsorbed at Au atom but if it is adsorbed at Ag atom, no synergistic effects are observed in terms of thermodynamical stability of TS, especially in ER pathways. The gold-palladium clusters are also good catalysts with low activation energy values and easy CO<sub>2</sub> dissociation, especially for LH pathways. This is because of a strong synergistic effects, especially in case of (Pd-C, Pd-O) reaction site. But in ER pathways, higher electronegativity of gold as compared to palladium reduces the observable synergistic effects, particularly for singly doped clusters. The gold-platinum clusters also show reasonable activation energy values and easy CO<sub>2</sub> dissociation for CO oxidation and seem as good catalysts for CO oxidation. They show good synergistic effects which becomes more evident when CO is adsorbed at Pt atom.

### 3.6. Adsorption and co-adsorption energetics

The catalytic active species in the cases studied here are not bare metal clusters, instead they are the adsorbed complexes which undergo further reaction with oxygen. Thus, study of adsorption and co-adsorption at various reaction sites becomes important to discuss the catalytic activity of a cluster.

Fig. 5 shows that there is a strong CO adsorption at Au, Pd and Pt sites for gold-silver trimers, gold-palladium trimers and gold-platinum trimers respectively. CO adsorption energies of singly doped trimers are found to be higher (more negative) than the doubly doped ones, except for gold-palladium trimers where their adsorption energies are comparable with a negligible difference of ~ and not approx. 2 kCal/mol. This shows that in case of gold-palladium trimers the CO adsorption is less composition dependent. The CO adsorption energy trend seen among the bimetallic trimers is as follows: Au-Ag bimetallic trimers (~ -20 kCal/mol) < Au-Pd bimetallic trimers (~ -40 kCal/mol) < Au-Pt bimetallic trimers (~ -50 kCal/mol). Most of the CO adsorbed complexes for bimetallic trimers are planar with the exceptions of two, one

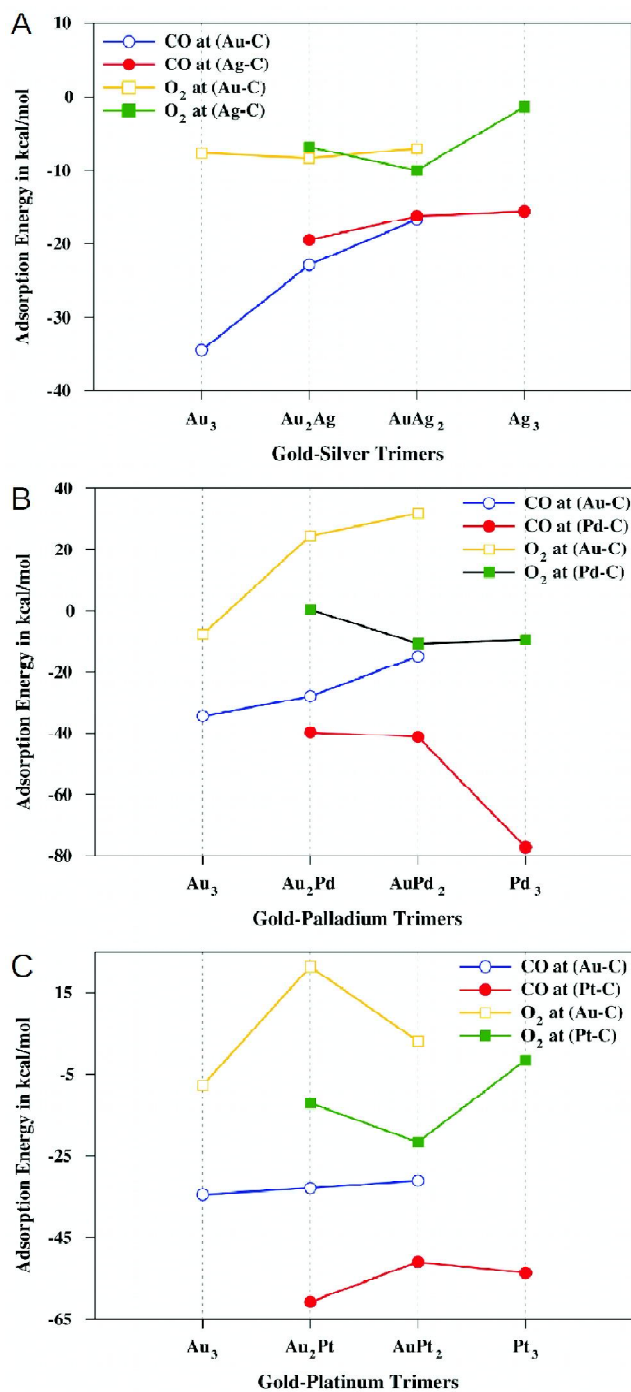


**Fig. 5.** The various CO and O<sub>2</sub> adsorption energies (in kcal/mol) for a cluster are marked in the plot with the x coordinate labelled by the cluster name. The various coloured lines show the qualitative aspects of CO and O<sub>2</sub> adsorption energy values for a particular adsorption site with increasing content of dopant in clusters. The different colours denote various possible adsorption sites.

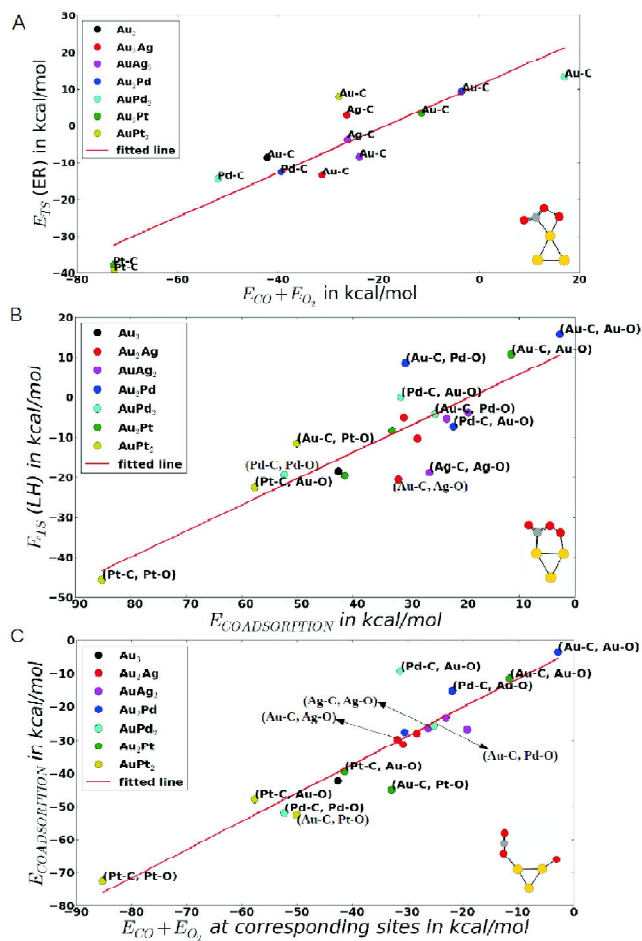


**Fig. 6.** Theoretical estimation of relative catalytic activities of different gold-based clusters in terms of adsorption energies. (A) Calculated ER transition state energies for adsorbed CO reacting with O<sub>2</sub> as a function of the sum of CO and O<sub>2</sub> adsorption energies.  $E_{TS}(ER) = 0.60 (E_{CO} + E_{O_2}) + 11.23 \text{ kcal/mol}$  and  $r^2 = 0.84$ . (B) Calculated LH transition state energies for adsorbed CO reacting with adsorbed O<sub>2</sub> as a function of the CO and O<sub>2</sub> co-adsorption energies.  $E_{TS}(LH) = 0.65 (E_{COadsorption}) + 12.36 \text{ kcal/mol}$  and  $r^2 = 0.74$ . (C) The scaling of the CO and O<sub>2</sub> co-adsorption energies with the sum of CO and O<sub>2</sub> adsorption energies.  $E_{COadsorption} = 0.86 (E_{CO} + E_{O_2}) - 2.99 \text{ kcal/mol}$  and  $r^2 = 0.84$ . Transition states for the reactions and co-adsorbed complex on gold-based trimers are shown as inserts.

AuPt<sub>2</sub> adsorption at Pt site and the other Au<sub>2</sub>Ag adsorption at Au site. Both of them have two possible geometries where CO bonds with both of the similar metal atoms but, the most stable structure of the two possibilities is the planar one. Among all the planar geometries of CO adsorbed complexes, AuPt<sub>2</sub> has the highest (most negative) CO adsorption energy.

Adsorption of O<sub>2</sub> is weaker than the CO adsorption for each cluster studied. O<sub>2</sub> adsorption energy increases (more negative) with addition of Y dopant, except for Au<sub>2</sub>Pd where O<sub>2</sub> adsorption is an endothermic process unlike others. O<sub>2</sub> adsorption energy of doped clusters is greater (more negative) than the monometallic clusters and is the highest (most negative) for doubly doped clusters. The O<sub>2</sub> adsorbed complexes on a few clusters also have two possible geometries, one O<sub>2</sub> bound to one atom of cluster and the other with O<sub>2</sub> bound to two similar metal atoms of cluster. The clusters AuAg<sub>2</sub> adsorption at Ag site, AuPd<sub>2</sub> adsorption at Pd site, AuPt<sub>2</sub> adsorption at Pt site, all prefer the first geometry as the most thermodynamically favorable. It can also be observed that O<sub>2</sub> adsorption is strongest at Au, Pd and Pt sites for Au<sub>2</sub>Ag, Au<sub>2</sub>Pd and Au<sub>2</sub>Pt respectively whereas, for doubly doped clusters it is strongest at Y site.

Positive linear correlations between transition state energies, E<sub>TS</sub> (ER) and E<sub>TS</sub> (LH), and the binding energies, E<sub>CO</sub> + E<sub>O<sub>2</sub></sub> and E<sub>coadsorption</sub>, are found for the bimetallic clusters with Pearson correlation coefficient of 0.92 and 0.86, respectively. A scaling between E<sub>coadsorption</sub> and E<sub>CO</sub> + E<sub>O<sub>2</sub></sub> is also found with 0.92 Pearson correlation coefficient. These relations are shown in Fig. 6. The linear relations for ER and LH transition state energies are quite similar and the gold-palladium trimers are closest to the top, followed by gold-silver clusters and gold-platinum clusters respectively.

#### 4. Conclusion

This paper presents a comprehensive theoretical study of CO oxidation reaction by unsupported bimetallic trimers in reference to pristine clusters, to give an understanding of engineering improved nanoalloy catalysts. This reaction on a bimetallic trimer can occur through a variety of different pathways, hence a careful choice of geometry of reaction intermediates is important. It was explored with two possible pathways for monometallic clusters whereas, five possible pathways for bimetallic clusters (two ER and three LH pathways). The catalytic active species for this case are the adsorbed and co-adsorbed complexes. Thus, the adsorption and reaction sites play a crucial role in the catalytic activity of bimetallic clusters for a reaction.

Bimetallic clusters show unique catalytic behavior based on the effect of second metal atom/s (dopant) added. The analysis reveals the composition-structure-activity relation-

ship of bimetallic clusters. CO oxidation reaction pathways on bimetallic clusters show less activation energy barrier, efficient O-O bond activation and easy CO<sub>2</sub> dissociation as compared to monometallic clusters. Hence, bimetallic clusters are believed to do better as compared to pure gold clusters as catalysts. Tweaking the level of interaction between the cluster metal atoms and the interaction between the catalyst cluster and the adsorbate molecules by adding suitable dopant metal atom/s in catalyst cluster is the key to tune the catalytic activity of a bimetallic nanoalloy cluster. We believe that this study offers a good theoretical understanding of designing efficient nanoalloys that can act as good catalysts for the CO oxidation reaction at ambient temperatures.

#### Acknowledgements

We thank DST-SERB (Grant No. EMR/2016/007697) for financial assistance. UDP thanks Professor Masahiro Ehara for his kind hospitality and Institute of Molecular Sciences, Japan for support via a Visiting Associate Professorship. SR thanks DST-Nano Mission for postdoctoral fellowship.

#### References

1. Masatake Haruta, Tetsuhiko Kobayashi, Hiroshi Sano and Nobumasa Yamada, *Chem. Lett.*, 1987, **16**, 405.
2. Olga Lopez-Acevedo, Katarzyna A. Kacprzak, Jaakko Akola and Hannu Häkkinen, *Nat. Chem.*, 2010, **2**, 329.
3. Manolis Stratakis and Hermenegildo Garcia, *Chem. Rev.*, 2012, **112**, 4469.
4. Dar Manzoor, Sailaja Krishnamurty and Sourav Pal, *Phys. Chem. Chem. Phys.*, 2016, **18**(10), 7068.
5. Dar Manzoor, Sailaja Krishnamurty and Sourav Pal, *J. Phys. Chem. C*, 2016, **120**(35), 19636.
6. Byoung Koun Min and Cynthia M. Friend, *Chem. Rev.*, 2007, **107**, 2709.
7. A. Stephen K. Hashmi and Graham J. Hutchings, *Angew. Chem. Int. Ed.*, 2006, **45**, 7896.
8. Pentti Frondelius, Hannu Häkkinen and Karoliina Honkala, *Phys. Rev. B*, 2007, **76**, 073406.
9. Steeve Chrétien, Steven K. Buratto and Horia Metiu, *Curr. Opin. Solid State Mater. Sci.*, 2007, **11**, 62.
10. Ajay M. Joshi, W. Nicholas Delgass and Kendall T. Thomson, *J. Phys. Chem. B*, 2006, **110**, 23373.
11. Mikael P. Johansson, Dage Sundholm and Juha Vaara, *Angew. Chem. Int. Ed.*, 2004, **43**, 2678.
12. Denisia M. Popolan, Melanie Nößler, Roland Mitrić, M. Bernhardt, Thorsten and Vlasta Bonačič-Koutecký, *Phys. Chem. Chem. Phys.*, 2010, **12**, 7865.
13. Ioannis N. Remediakis, Nuria Lopez and Jens K. Nørskov,

- Angew. Chem. Int. Ed.*, 2005, **117**, 1858.
14. T. V. Choudhary and D. W. Goodman, *Top. Catal.*, 2002, **21**, 25.
  15. Heemin Yoo, "Interfacial structure and dynamics of nematic 4-n-pentyl-4'-cyanobiphenyl liquid crystals on silver, silica and modified silica substrates", The University of Arizona, 2009.
  16. Sandhya Rai, Masahiro Ehara and U. Deva Priyakumar, *Phys. Chem. Chem. Phys.*, 2015, **17**, 24275.
  17. Andrew A. Herzing, Christopher J. Kiely, Albert F. Carley, Philip Landon and Graham J. Hutchings, *Science*, 2008, **321**, 1331.
  18. Liana D. Socaciu, Jan Hagen, Thorsten M. Bernhardt, Ludger Wöste, Ulrich Heiz, Hannu Häkkinen and Uzi Landman, *J. Am. Chem. Soc.*, 2003, **125**, 10437.
  19. Lars Grabow, Ye Xu and Manos Mavrikakis, *Phys. Chem. Chem. Phys.*, 2006, **8**, 3369.
  20. M. J. Lippits, A. C. Gluhoi and B. E. Nieuwenhuys, *Top. Catal.*, 2007, **44**, 159.
  21. Lu Gang, B. G. Anderson, J. Van Grondelle and R. A. Van Santen, *Appl. Catal. B: Environ.*, 2003, **40**, 101.
  22. Jan Hagen, Liana D. Socaciu, Jérôme Le Roux, Denisia Popolan, Thorsten M. Bernhardt, Ludger Wöste, Roland Mitrić, Holger Noack and Vlasta Bonacić-Koutecký, *J. Am. Chem. Soc.*, 2004, **126**, 3442.
  23. Dianyong Tang, Zhongzhu Chen, Jianping Hu, Guofeng Sun, Shenzhuang Lu and Changwei Hu, *Phys. Chem. Chem. Phys.*, 2012, **14**, 12829.
  24. Jia Zhou, Zhen-Hua Li, Wen-Ning Wang and Kang-Nian Fan, *J. Phys. Chem. A*, 2006, **110**, 7167.
  25. U. Heiz, A. Sanchez, S. Abbet and W.-D. Schneider, *J. Am. Chem. Soc.*, 1999, **121**, 3214.
  26. C. Becker and C. R. Henry, *Catal. Lett.*, 1997, **43**, 55.
  27. Denisia M. Popolan, Melanie Nossler, Roland Mitrić, Thorsten M. Bernhardt and Vlasta Bonačić-Koutecký, *J. Phys. Chem. A*, 2011, **115**, 951.
  28. Dong Die, Ben-Xia Zheng, Lan-Qiong Zhao, Qi-Wen Zhu and Zheng-Quan Zhao, *Sci. Rep.*, 2016, 6.
  29. Natalia Palina, Osami Sakata, LSR Kumara, Chulho Song, Katsutoshi Sato, Katsutoshi Nagaoka, Tokutaro Komatsu, Hirokazu Kobayashi, Kohei Kusada and Hiroshi Kitagawa, *Sci. Rep.*, 2017, **7**, 41264.
  30. Yanbiao Wang, Guangfen Wu, Mingli Yang and Jinlan Wang, *J. Phys. Chem. C*, 2013, **117**, 8767.
  31. Jun-Hong Liu, Ai-Qin Wang, Yu-Shan Chi, Hong-Ping Lin and Chung-Yuan Mou, *J. Phys. Chem. B*, 2005, **109**, 40.
  32. Dennis Palagin and Jonathan P. K. Doye, *Phys. Chem. Chem. Phys.*, 2015, **17**, 28010.
  33. Thorsten M. Bernhardt, Liana D. Socaciu-Siebert, Jan Hagen and Ludger Wöste, *Appl. Catal. A*, 2005, **291**, 170.
  34. Yasuo Iizuka, Aya Kawamoto, Kazuhiro Akita, Masakazu Daté, Susumu Tsubota, Mitsutaka Okumura and Masatake Haruta, *Catal. Lett.*, 2004, **97**, 203.
  35. Fabio R. Negreiros, Luca Sementa, Giovanni Barcaro, S Vajda, Edoardo Apra and Alessandro Fortunelli, *ACS Catal.*, 2012, **2**, 1860.
  36. Fang Wang, Dongju Zhang and Yi Ding, *J. Phys. Chem. C*, 2010, **114**, 14076.
  37. Yoko Abe, Kei Kuramoto, Masahiro Ehara, Hiroshi Nakatsuji, Michinori Suginome, Masahiro Murakami and Yoshihiko Ito, *Organometallics*, 2008, **27**, 1736.
  38. Sumanta Kumar Padhi, Ryoichi Fukuda, Masahiro Ehara and Koji Tanaka, *Inorg. Chem.*, 2012, **51**, 5386.
  39. Yoshimasa Makita, Keisuke Ikeda, Kazuya Sugimoto, Tomoyuki Fujita, Tomofumi Danno, Karan Bobuatong, Masahiro Ehara, Shin-ichi Fujiwara and Akiya Ogawa, *J. Organomet. Chem.*, 2012, **706**, 26.
  40. Tao Yang, Ryoichi Fukuda, Saburo Hosokawa, Tsunehiro Tanaka, Shigeyoshi Sakaki and Masahiro Ehara, *Chem. Cat. Chem.*, 2017, **9**, 1222.
  41. Hanne Falsig, Britt Hvolbæk, Iben S. Kristensen, Tao Jiang, Thomas Bligaard, Claus H. Christensen and Jens K. Nørskov, *Angew. Chem. Int. Ed.*, 2008, **120**, 4913.
  42. Aditi Gupta, Bundet Boekfa, Hidehiro Sakurai, Masahiro Ehara and U. Deva Priyakumar, *J. Phys. Chem. C*, 2016, **120(31)**, 17454.
  43. Masahiro Ehara and U. Deva Priyakumar, *Chem. Rec.*, 2019.
  44. Nuria Lopez, T. V. W. Janssens, B. S. Clausen, Y. Xu, Manos Mavrikakis, T. Bligaard and Jens Kehlet Nørskov, *J. Catal.*, 2004, **223**, 232.
  45. Ton V. W. Janssens, Bjerne S. Clausen, Britt Hvolbæk, Hanne Falsig, Claus H. Christensen, Thomas Bligaard and Jens K. Nørskov, *Top. Catal.*, 2007, **44**, 15.
  46. Caixia Xu, Jixin Su, Xiaohong Xu, Pengpeng Liu, Hongjuan Zhao, Fang Tian and Yi Ding, *J. Am. Chem. Soc.*, 2007, **129**, 42.
  47. Birte Jürgens, Christian Kübel, Christian Schulz, Tobias Nowitzki, Volkmar Zielasek, Jürgen Biener, Monika M. Biener, Alex V. Hamza, and Marcus Bäumer, *Gold Bull.*, 2007, **40**, 142.
  48. Yan-Xia Zhao, Qing-Yu Liu, Mei-Qi Zhang and Sheng-Gui He, *J. Chem. Soc., Dalton Trans.*, 2016, **45**, 11471.
  49. Neetu Goel, "Chemical Modelling", Vol. 14, Royal Society of Chemistry, 2018.
  50. Mark D. Levin, David M. Kaphan, Cynthia M. Hong, Robert G. Bergman, Kenneth N. Raymond and F. Dean Toste, *J. Am. Chem. Soc.*, 2016, **138**, 9682.
  51. Filip Zasada, Janusz Janas, Witold Piskorz, Magdalena Gorczynska and Zbigniew Sojka, *ACS Catal.*, 2017, **7**, 2853.
  52. Liang Wang, Jian Zhang, Yihan Zhu, Shaodan Xu, Chengtao Wang, Chaoqun Bian, Xiangju Meng and Feng-Shou Xiao

Gurtu *et al.*: Comparative study of the efficiency of Au, Ag, Pd and Pt based mono and bimetallic trimer clusters *etc.*

- ACS Catal., 2017, **7**, 7461.
53. Zhi-Pan Liu, P. Hu and Ali Alavi, *J. Am. Chem. Soc.*, 2002, **124**, 14770.
54. Nuria Lopez and Jens K. Nørskov, *J. Am. Chem. Soc.*, 2002, **124**, 11262.
55. Chun Zhang, Bokwon Yoon and Uzi Landman, *J. Am. Chem. Soc.*, 2007, **129**, 2228.
56. Ye Xu and Manos Mavrikakis, *J. Phys. Chem. B*, 2003, **107**, 9298.
57. Zhi-Pan Liu, Xue-Qing Gong, Jorge Kohano, Cristián Sanchez and Peijun Hu, *Phys. Rev. Lett.*, 2003, **91**, 266102.
58. Carlos Gonzalez and H. Bernhard Schlegel, *J. Phys. Chem.*, 1990, **94**, 5523.
59. Hannu Häkkinen, Michael Moseler and Uzi Landman, *Phys. Rev. Lett.*, 2002, **89**, 033401.
60. Hannu Häkkinen and Uzi Landman, *J. Am. Chem. Soc.*, 2001, **123**, 9704.
61. Saumya Gurtu, Sandhya Rai, Masahiro Ehara and U. Deva Priyakumar, *Theor. Chem. Acc.*, 2016, **135**, 1.
62. John P. Perdew, Kieron Burke and Matthias Ernzerhof, *Phys. Rev. Lett.*, 1996, **77**, 3865.
63. John P. Perdew, Kieron Burke and Yue Wang, *Phys. Rev. B*, 1996, **54**, 16533.
64. L.-L. Wang and D. D. Johnson, *J. Phys. Chem. B*, 2005, **109**, 23113.
65. Joachim Paier, Martijn Marsman and Georg Kresse, *J. Chem. Phys.*, 2007, **127**, 024103.
66. Carlo Adamo and Vincenzo Barone, *Theor. Chem. Acc.*, 2000, **105**, 169.
67. Alessandro Stroppa, Konstantinos Termentzidis, Joachim Paier, Georg Kresse and Jürgen Hafner, *Phys. Rev. B*, 2007, **76**, 195440.
68. Gaussian 09, revision a, Inc, Wallingford CT, 2009.
69. A. W. Ehlers, M. Böhme, S. Dapprich, A. Gobbi, A. Höllwarth, V. Jonas, K. F. Köhler, R. Stegmann, A. Veldkamp and G. Frenking, *Chem. Phys. Lett.*, 1993, **208**, 111.
70. M. Dolg, U. Wedig, H. Stoll and H. Preuss, *J. Chem. Phys.*, 1987, **86**, 866.
71. Eva M. Fernández, José M. Soler and Luis C. Balbás, *Phys. Rev. B*, 2006, **73**, 235433.
72. Jan M. L. Martin and Andreas Sundermann, *J. Chem. Phys.*, 2001, **114**, 3408.
73. Behnam Assadollahzadeh and Peter Schwerdtfeger, *J. Chem. Phys.*, 2009, **131**, 064306.
74. Xiaoyan Cao and Michael Dolg, *J. Chem. Phys.*, 2001, **115**, 7348.
75. Xiaoyan Cao and Michael Dolg, *J. Mol. Struct.*, 2004, **673**, 203.
76. W. Küchle, M. Dolg, H. Stoll and H. Preuss, *Mol. Phys.*, 1991, **74**, 1245.
77. D. W. Yuan, Yang Wang and Zhi Zeng, *J. Chem. Phys.*, 2005, **122**, 114310.
78. AliMAbdel-Mageed, Bunyarat Rungtaweevoranit, Magdalena Parlinska-Wojtan, Xiaokun Pei, Omar M Yaghi and R. Jürgen Behm, *J. Am. Chem. Soc.*, 2019.
79. Xue Feng, Lixia Ling, Yueting Cao, Riguang Zhang, Maohong Fan and Baojun Wang, *J. Phys. Chem. C*, 2018, **122**, 1169.
80. R. Mitrić, C. Bürgel, J. Burda, V. Bonačić-Koutecký and P. Fantucci, *Eur. Phys. J.*, 2003, **D24**, 41.
81. Naresh K. Jena, K. R. S. Chandrakumar and Swapan K. Ghosh, *J. Phys. Chem. C*, 2012, **116**, 17063.

